Journal of Brilliant Engineering 4 (2024) 4949

Brilliant Engineering

journal home: www.acapublishing.com/journals/4/ben

Research Article

Impact of Natural Disasters on Flooding: An Assessment Using Satellite Data and Surface-Subsurface Modeling

Hafiz Ahmad*,[1], Wiley Vickers[2]

[1]Teaching Professor, Department of Civil and Environmental Engineering, Florida State University- Panama City, USA.

[2]MS Student, Department of Civil and Environmental Engineering, Florida State University- Panama City, USA.

Keywords

Flood inundation, Hurricane Michael, ICPR, Imagery, Surface water-groundwater interaction model.

Abstract

Dealing with large watersheds sometimes becomes challenging, especially when simulating the surface water-groundwater (SW-GW) interaction within the floodplain. Using satellite data (such as land cover, topography, bathymetry, soil zones, imagery, etc.) can be an excellent way to characterize the surface and subsurface properties to handle large basins, especially those suffering drastic changes due to natural disasters. This study employs satellite data from 2016 and 2019 to develop integrated SW-GW models, aiming to assess the impacts of changes in basin characteristics on surface-subsurface hydrology and flooding. The model was then used to evaluate the flooding impact due to Hurricane Michael (of 2018) in a 437 km2 watershed. Satellite data showed significant changes in hydrologic conditions including tree loss in the study area due to Hurricane Michael. Results for a 25-year 24-hour storm show a 256% increase in flood inundation areas due to the impact of Hurricane Michael. The model could pinpoint locations vulnerable to flooding due to the change in the hydrologic condition of the watershed. Among the 92,206 nodes generated by the model, the most vulnerable flooding location showed 1.9 m excess flooding in the post-hurricane affected area compared to its pre-hurricane condition. Additionally, the SW-GW model accurately tracked stage changes at a gauge station during a 2.5-hour (54.6 mm) storm in March 2022.

1. Introduction

Frequent flooding poses a major hazard to urban growth in many regions across the globe, including developed nations. Understanding the underlying scientific causes of increasingly frequent and intense flooding—particularly following major natural disasters such as hurricanes—is critical for researchers and city planners. This knowledge is essential for improving flood forecasting implementing effective flood management and mitigation strategies. In addition, pinpointing flood-prone areas, assessing the extent of inundation, estimating the time to reach specific inundation levels, and quantifying runoff volumes associated with storm events are crucial steps in addressing these hazards effectively.

Historically, one-dimensional (1D) hydraulic models have been used for simulating runoff and flood dynamics [1]. However, these models have limitations, especially in simulating the interaction between surface water and groundwater (SW-GW) within floodplains, which is essential for accurately predicting flood depth and extent [2]. Groundwater fluctuations, subsurface saturation, and land surface conditions can significantly amplify flooding, even from relatively low-intensity storms.

Recent advancements in flood modeling have seen the development of two-dimensional (2D) hydrodynamic models, as well as improved 1D models, to generate more accurate flood inundation maps for both small and large watersheds [3, 4, 5, 6, 7]. Despite these developments, there remains a gap in research evaluating the causes of flooding in areas impacted by natural disasters, such as hurricanes. Furthermore, integrating modern satellite imagery and related data into hydrologic models, particularly for understanding SW-GW interactions, remains a challenge. Researchers often face difficulties in incorporating these complex datasets into hydraulic models, which can be time-consuming and technically demanding.

In recent years, Bay County, Florida, USA, has become increasingly vulnerable to flooding, particularly after Hurricane Michael in 2018. Even minimal rainfall in certain neighborhoods leads to severe inundation, affecting residents and businesses alike. This study aims to develop an integrated surface-water and groundwater (SW-GW) model using ICPR 4 software to provide a scientific explanation for these persistent flooding issues. Specifically, this study seeks to:

- Assess how Hurricane Michael altered surface and subsurface hydrology, with a particular focus on its impact on flood dynamics.
- Demonstrate the process of integrating satellite imagery and related data into the SW-GW hydrologic model.
- Identify vulnerable areas and pinpoint flood-prone regions within the watershed, both before and after the hurricane.
- Quantify flood inundation severity by comparing model-predicted flood scenarios with actual observed events post-Hurricane Michael.

This research is expected to produce detailed flood inundation maps that will be invaluable for city planners and policymakers in designing effective flood mitigation strategies and land-use planning decisions. Moreover, by exploring modern techniques for integrating satellite imagery and spatial data into hydraulic models, the study offers the research community valuable tools to improve the accuracy and reliability of flood predictions, which will ultimately aid in better flood management and resilience planning.

*Corresponding Author: hahmad@pc.fsu.edu
Received 03 Oct 2024; Revised 05 Jan 2025; Accepted 05 Jan 2025

https://doi.org/10.36937/ben.2024.4949

2. Study Area

The site selected for this study is the Beer Creek Watershed, which spans 437 km^2 (169 mi^2) in Bay County, Florida, USA. Figure 1 shows the delineation of the watershed area analyzed in this study, highlighting the key features relevant to the flood modeling process. This area experienced catastrophic damage from Hurricane Michael, a Category 5 storm, on October 10, 2018. The hurricane caused significant changes to the hydrology of the watershed. To characterize the conditions before and after Hurricane Michael, the initial step involved acquiring data on the watershed.

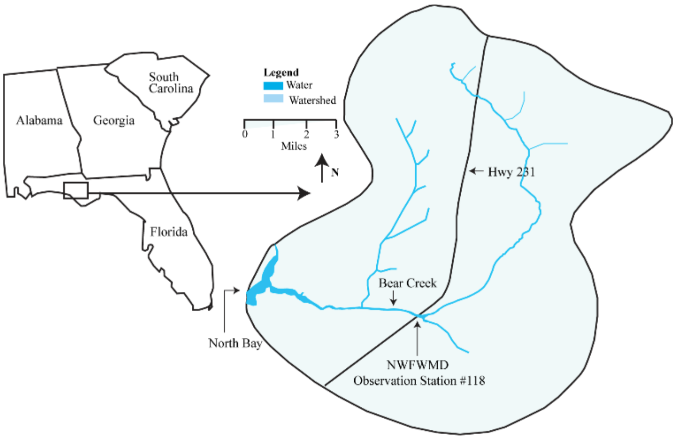

Figure 1. Watershed boundary and study area

3. Data acquisition

The hydrologic data of 2016 (before the hurricane) and 2022 (after the hurricane) were used as input to develop an SW-GW integrated model. This data can be categorized into three basic components: the surface system, the vadose zone, and the saturated groundwater system. Figure 2 shows the schematic diagram that depicts the processes governing the interaction between surface water and groundwater, essential for understanding flood dynamics in the study area. This Figure also illustrates the sources of these three categories of data.

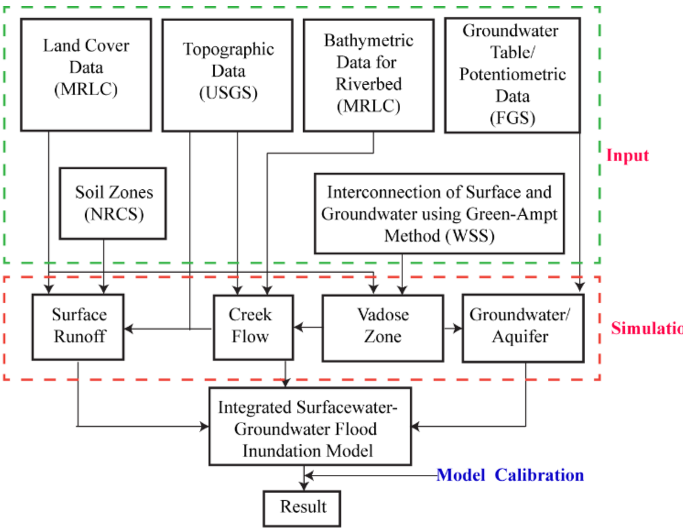

Figure 2. Schematic diagram illustrating the interaction between surface water (SW) and groundwater (GW) in floodplains.

3.1. Satellite and Geospatial Data Processing and Integration into the Model

Satellite and geospatial data, including topographic, bathymetric, land cover, and imperviousness data, were integral to developing the model for the Bear Creek basin. The process involved several steps to ensure that these data sources were properly prepared and integrated for modeling purposes.

3.1.1. Land cover data

Land cover and imperviousness data were crucial for the hydrological modeling as seen in Figure 2. These datasets were obtained from the MRLC Interactive Data Viewer, specifically the 2016 and 2019 CONUS Land Cover and Impervious Surface datasets (https://www.mrlc.gov/viewer/), which are available as GeoTIFF raster files. These files were processed using ArcGIS, where the first task was to convert the raster data into polygons using the "Raster to Polygon" tool, making the data compatible for integration into the ICPR model.

The data underwent several preprocessing steps. First, the coordinate system was adjusted to align with the existing DEM data, ensuring spatial consistency. The datasets were also classified by land cover type, and the percentage of impervious surface within each land cover zone was calculated using the "Summarize Within" tool in ArcGIS. This tool allowed us to summarize the imperviousness within each land cover polygon, providing a detailed map of impervious areas that could influence runoff.

The land cover and imperviousness data were then imported into the ICPR model. For the imperviousness data, additional calculations were made to estimate the Directly Connected Impervious Area (DCIA), using the Sutherland Equations to estimate the effective impervious area (EIA) connected to the outlet of the basin. This calculation was essential for simulating runoff in the model, as it accounts for the connectivity of impervious surfaces to the hydrological system. Table 1 presents the land cover data for 2016 (before) and 2019 (after) Hurricane Michael

Table 1. Change of land-cover data

Description	2016 area (km^2)	2019 area (km^2)	Change (km^2)	2016 CN	2019 CN
Open Water	2.54	1.98	-0.56	100	100
Dev, Open space	21.51	21.00	-0.52	69	69
Dev, low int	8.38	8.49	0.12	70	70
Dev, med int	1.54	1.96	0.43	85	85
Dev, high int	0.14	0.19	0.05	92	92
Barren land	1.31	1.52	0.21	86	86
Deciduos forest	0.26	0.55	0.29	55	55
Evergreen forest	124.77	105.62	-19.15	55	55
Mixed forest	0.02	0.31	0.29	55	55
Shrub	70.34	80.39	10.05	48	67
Grassland	54.08	62.35	8.27	61	61
Pasture/Hay	3.62	3.59	-0.03	61	61
Cultivated crop	5.24	5.36	0.12	58	65
woody wetlands	135.00	128.73	-6.28	100	100
wetlands	8.47	15.17	6.70	100	100
Total Area (km^2)	437.2	437.2			

3.1.2. Surface topography

The surface topography of the Bear Creek basin was characterized using the most recent 1-meter Digital Elevation Models (DEMs) derived from LiDAR surveys. These LiDAR-derived DEMs were obtained from the USGS 3DEP Lidar Explorer (https://apps.nationalmap.gov/lidar-explorer/#/). Since the DEMs are raster data files, the first step involved importing them into ArcGIS Pro, where they were processed for use in the ICPR model.

The DEMs from the LiDAR surveys were initially large and required combining multiple files into a single, continuous raster layer. This was achieved using the "Mosaic to New Raster" tool in ArcGIS, which allowed for the stitching of the DEM files into a unified surface model. The DEM was then clipped to the boundary of the Bear Creek basin using a rectangular polygon drawn to define the basin's limits.

3.1.3. Bathymetric data

During the processing of the DEM (mentioned above), it was noted that no significant bathymetric data was available for areas with significant water depth. This was a limitation inherent to standard LiDAR technology, which uses infrared lasers that either get absorbed or refracted in water, thus missing bathymetric data in these regions. To address this gap, bathymetric data was sourced from NOAA's National Centers for Environmental Information (NCEI)(https://www.ncei.noaa.gov/maps/bathymetry/), specifically from the Continuously Updated Digital Elevation Model (CUDEM) dataset, which provides bathymetric data at a 9th arc second resolution.

The bathymetric data was processed in the same manner as the topographic data. It was imported into ArcGIS Pro, and the "Mosaic to New Raster" tool was again used, but with the mosaic operator set to "minimum" to preserve the LiDAR topographic values while integrating the bathymetric values in deeper areas. This method ensured that the bathymetric data, which typically represents lower elevations, did not overwrite the topographic data but instead supplemented it in water bodies and deeper regions. The final integrated DEM was then prepared for use in the ICPR model.

3.2. Groundwater data

Initially, potentiometric data for groundwater were obtained from the Florida Geological Survey (FGS) (https://fdep.maps.arcgis.com/apps/webappviewer). However, this data was found to be unrepresentative of the current water table, as it significantly differed from field measurements. Consequently, a water table surface was created by subtracting the average water table depth, obtained from the USGS Web Soil Survey, from the topographic DEM.

3.3. Soil zones data

The soil zones and physical characteristic data needed for the Green-Ampt method (discussed later) were obtained from the USGS Web Soil Survey (https://websoilsurvey.sc.egov.usda.gov/App/WebSoilSurvey.aspx). To extract the data, a shapefile was used, and the process was streamlined by employing the rectangular boundary shapefile of the topographic DEM. The area was divided into three equal-sized sections using the Split tool in ArcGIS to circumvent the web soil survey's maximum allowable area size and the boundary defined by the shapefile. Each section was imported into the web soil survey, and its soil data were downloaded. Within the soil data, there was a shapefile for each section. These three shapefiles were then imported into ArcGIS and merged using the Merge tool. Finally, the resulting polygon dataset was processed with the Dissolve Boundaries tool, which merged adjacent polygons with the same properties into a single polygon, based on the mukey value—an identification number for the soil type within each polygon.

4. Hydrologic Model Development

4.1. ICPR program

Given the need to integrate surface runoff with subsurface hydrology over a relatively large watershed (437 km^2), the ICPR (v.4) software from Streamline Technologies [8] was deemed the most suitable for this study. ICPR is a FEMA-approved tool capable of developing both hydraulic and hydrologic models. It has been extensively validated for surface water and groundwater simulation in numerous watersheds across Florida, USA [7, 9, 10].

4.1.1. Surface runoff

Details about this software, including its functionality and the relevant equations used for hydrologic and hydraulic simulations, can be found elsewhere [7,8]. In summary, the program generates flexible triangular computational meshes based on the topographic Digital Elevation Model (DEM) and other surface features, such as breakpoints. The vertices of these triangles serve as nodes within the model, while the sides of the triangles represent overland flow links, facilitating 2D overland flow between adjacent vertices. ICPR employs several methods to calculate flow rates, with the energy equation combined with the continuity equation being commonly used for runoff simulation (as shown below):

$$Q=\left\{\frac{Z_1\text{-}Z_2}{\frac{1}{2g}\left[\frac{1}{A_2^2}\text{-}\frac{1}{A_1^2}\right]+\Delta x C_f}\right\}^{1/2}$$

Where Q= volumetric flow rate; Z_1 = surface water elevation head at the upstream node; Z_2 = surface water elevation head at the downstream node; g= acceleration due to gravity; A_2= cross-sectional area at the downstream node; A_1 = cross-sectional area at the upstream node; Δx = distance in flow direction; and C_f = conveyance factor.

Control volumes are created around the vertices, extending to the midpoints of the triangle sides and the geometric center of the triangle (e.g., the centroid), resulting in a honeycomb-like structure. This honeycomb mesh represents the hydrologic elements of the model. Subsequently, a diamond-shaped polygon is generated around each flow link, characterized by roughness coefficients and the average ground slope. Water flows from one control volume to an adjacent control volume via the overland flow links or triangle sides.

4.1.2. Sub-surface flow simulation

For the 2D groundwater simulation, ICPR employs a finite element approach similar to the one used for 2D overland flow, utilizing the same triangular mesh. However, in the groundwater simulation, nodes are placed at the midpoints of the triangle sides. A polygonal honeycomb structure is then generated around these nodes. The groundwater flow is modeled by solving the continuity equation, as shown below, applied across the entire mesh.

$$n\frac{\partial h}{\partial t}=-\frac{\partial(uh)}{\partial x}-\frac{\partial(vh)}{\partial y}$$

where n=fillable porosity; h=groundwater elevation; u and v=velocity vector components; t=time; and x and y=cartesian coordinates. The two honeycomb structures are then overlapped and intersected by the vadose zone, creating sub-polygons or soil cylinders. This process transfers excess rainfall from the surface honeycomb to the groundwater honeycomb through infiltration or seepage.

4.1.3. Surface and subsurface interaction

Water accumulates when multiple soil cylinders share the same surface node. These cylinders are then shifted horizontally along the triangle edges, generating surface runoff. If the water in a soil cylinder crosses the interface between the vadose and saturated zones, it is transferred to the corresponding groundwater node. When a soil cylinder becomes saturated, the surface becomes inundated.

4.2. Model Development

The development of the hydraulic model using ICPR began with creating a scenario in which all surfaces and map layers (as discussed in Section 3) were incorporated into the ground meshes, including any specific points or lines. For this process, surfaces such as DEMs or raster files and map layers, such as polygon shapefiles, were imported. In the map layers' section, raster data was generated and regions were defined, resulting in two types of regions: overland flow and groundwater flow regions. Both types of regions were set up using similar processes. Map layers and surfaces were then defined, and the mesh settings were configured. This study employed a minimum angle of 21 degrees, a minimum area of 14 m² (150 ft²), a maximum area of 13936 m² (150,000 ft²), a boundary spacing of 305 m (1,000 ft), and a cell or mesh size of 0.1 m² (1 ft²).

Once the surfaces and data were integrated into the model, initial conditions were established by placing boundary stage nodes in downstream and upstream areas where data was available. These points were assigned specific stages based on observed gage station data to control ponding at the boundary of the overland flow region. ICPR interprets these boundaries as vertical walls that do not allow water to pass through. A 2-day simulation was then performed, and the resulting elevation was used to create a preliminary initial stage surface to help the groundwater achieve a steady-state (SS) condition. The SS condition was reached through a 1-month simulation, during which time series data were analyzed to determine when the depth change was minimized. The elevation at that point became the new groundwater surface.

Subsequently, the actual test storm event was simulated separately later in the procedure. This was necessary due to the method used to generate the SS groundwater surface. The stage was simulated again to observe its reaction to the new water table. The only difference in this simulation was that the water table for the pre-condition was artificially lowered by 0.76 m (2.5 ft) to reflect the change from 2018 pre-hurricane conditions to 2022 post-hurricane conditions, as the data used in the model was from October 2022. (Figure 3). This adjustment was based on the difference in the average groundwater elevation in April from an observation well (Location: 005950, Name: TRAPP POND) of the NWFWMD (https://nwfwmd.aquaticinformatics.net/). Figure 3 shows the temporal variation in the groundwater table levels at the TRAPP POND monitoring well, illustrating the impact of different storm events on subsurface hydrology. As shown in this Figure, the groundwater observation well from April 2018 had an average elevation that was 0.76 m lower than the average elevation in each subsequent April.

The integration of surface and groundwater interconnections was accomplished using the refined Green-Ampt method. As part of this method, each soil column was assigned a depth of 6.1 m (20 ft) and divided into cells with a thickness of 0.06 m (1/5 ft). To calculate the Green-Ampt parameters, the method requires the soil zones to be defined and physical characteristic data to be provided. The polygon maps created for the model's soil zones (described in Section 3.4) were imported into the ICPR model. Data associated with each soil zone was imported using a method published by Streamline Technologies [8] that is included with ICPR.

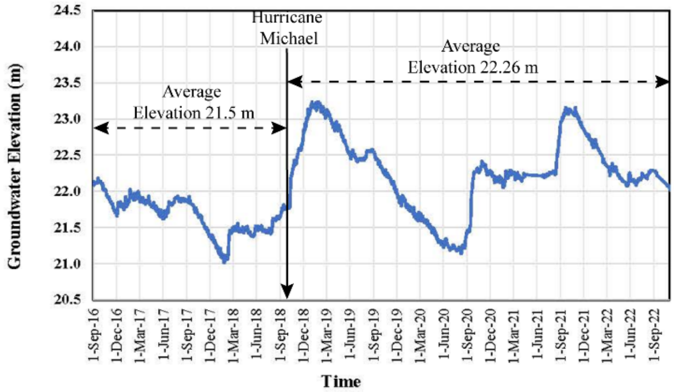

Figure 3. Variation of groundwater table at TRAPP POND monitoring well over time.

5. Results

5.1. Pre-and post-hurricane flood conditions

To better understand the impact of Hurricane Michael on hydrological conditions, a comparison between pre- and post-hurricane flood conditions was conducted using the NRCS runoff curve number (CN) method. This method allowed for the quantification of runoff based on land cover changes, which were significant in this case due to the hurricane's destruction of forested areas.

Before Hurricane Michael, the watershed was primarily covered by mature evergreen forests, which are highly effective at intercepting rainfall and reducing runoff due to their dense canopy and deep root systems. After the storm, these forests were replaced with shrubland, a less dense land cover type with a lower capacity to absorb rainfall. This shift in vegetation contributed to an increase in surface runoff, as shrubland provides significantly less water retention capacity compared to mature forests. This change in land cover was directly reflected in the higher CN values assigned to the post-hurricane conditions (shrubland and cultivated crops), which resulted in increased runoff potential [10].

Using the land cover maps from 2016 and 2019, we applied the CN values derived from Technical Release 55 [11] and shown in Table 1. For the post-hurricane conditions, shrubland and cultivated crops were assigned higher CN values to reflect the less dense nature of young shrubland and the change from mature pine forests. These higher CN values represent increased runoff potential.

The total runoff volume for the post-hurricane scenario was quantified at 8,078 ha-m (785,842 ac-in) using NRCS equations [11]. This runoff volume is significantly higher than the pre-hurricane runoff volume of 7,551 ha-m (734,557 ac-in). This increase (527 ha-m) is primarily attributed to the loss of evergreen forests and the subsequent replacement by shrubland. As a result, the basin now produces more runoff, which could lead to higher flood risks and challenges for water management in the affected areas.

5.2. Flood-prone areas

The watershed initially had a submerged area of 35 km². This area primarily included Bear Creek, its tributaries, and Deer Point Lake, into which Bear Creek flows. To assess the flood-prone areas within the watershed, a 25-year, 24-hour design storm (267 mm of rainfall) was used for simulation. The simulation revealed that the storm could inundate 49.7 km² of the watershed (pre-hurricane condition, 2016). This indicated an increase in inundation of 14.7 km² (A_{pre}) due to the storm event.

On the other hand, approximately 87.5 km² were inundated due to the same storm in the post-hurricane scenario (2022). This represents an increase of 52.4 km² (A_{post}) compared to the submerged area before the design storm. Consequently, there is a 256% increase in inundation, as calculated using the equation below, due to the altered hydrologic conditions caused by Hurricane Michael. Figure 4 compares the flood-prone areas in the watershed both before and after Hurricane Michael, highlighting changes in inundation patterns due to the storm's impact. The submerged areas (shown in blue color) are generated by the model for the 25-year, 24-hour storm event.

$$\text{Increase (\%)} = \frac{(A_{\text{Post}} - A_{\text{Pre}})}{A_{\text{Pre}}} \text{x}100\%$$

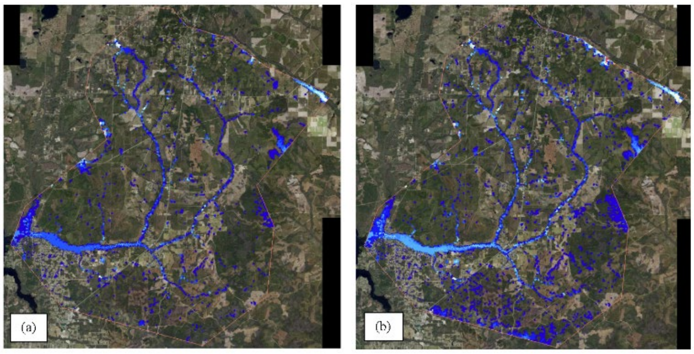

Figure 4. Flood-prone areas identified pre- and post-Hurricane Michael: (a) Pre-hurricane conditions (24 hours after the storm, (b) Post-hurricane conditions (24 hours after the storm).

The larger flooded area suggests that post-hurricane conditions are more prone to flooding under similar storm events, indicating a significant shift in the watershed's hydrological behavior. The substantial increase in inundation highlights the lasting effects of the storm on local flood risk. The simulation results shown in Figure 4 provide a clear visual representation of the changes in inundation patterns, demonstrating how the same storm event affected the watershed differently before and after the hurricane.

5.3. Pinpointing vulnerable locations

ICPR generated 92,206 nodes to identify the locations most vulnerable to flooding using the 25-year, 24-hour design storm. Figure 5 illustrates the inundation depths for both pre- and post-hurricane conditions, and shows the differences in flooding severity as a result of Hurricane Michael for a 25-year, 24-hour storm. It presents the simulated results for the top five flooding locations or nodes (ranked #1 through #5 in descending order) where the maximum stage change for the post-hurricane condition (2022) can occur. These stage changes were calculated relative to the initial condition. For example, the most vulnerable location (#1) was at 85.43°W, 30.37°N, where the stage increased by 1.8 m (5.79 ft) for the pre-hurricane condition (2016) compared to the initial condition. At the same location, the post-hurricane (2022) stage rise was 3.6 m (11.92 ft) from the initial condition, representing an excess of 1.83 m (6.13 ft) of flooding compared to the pre-hurricane condition (2016). Similarly, stage changes for the pre-and post-hurricane conditions are determined and plotted in Figure 5 for other locations. In all cases, post-hurricane flood inundation (i.e., excess flooding) exceeded that of the pre-hurricane condition.

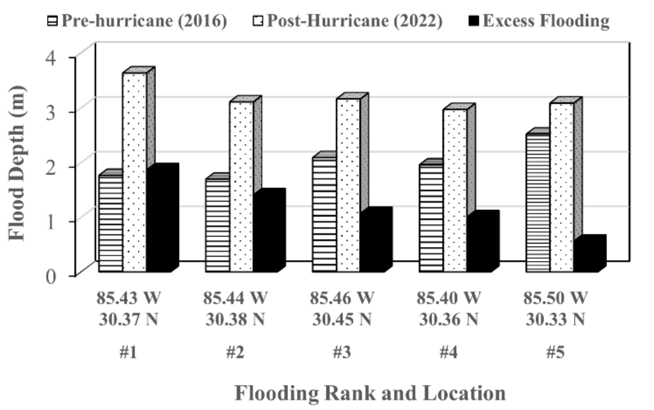

Figure 5. Inundation depths for Pre- and Post-hurricane conditions and their differences during the 25-year 24-hour storm events

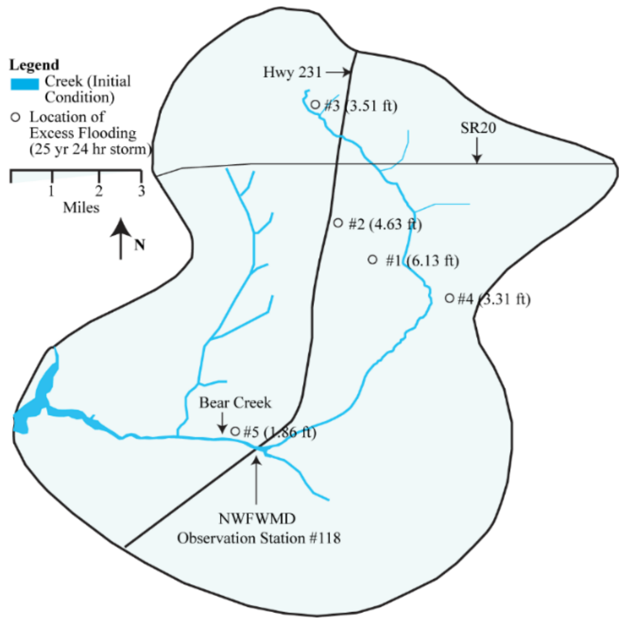

Figure 6. Maximum flooding locations within the study area

As seen in Figure 5, these findings were consistent across multiple locations, confirming that the post-hurricane conditions resulted in more severe flooding in most of the watershed. The identification of these flood-prone hotspots is critical for future flood management and can inform targeted mitigation strategies, such as improving stormwater infrastructure in these high-risk areas.

As mentioned, the model could also pinpoint the locations vulnerable to flooding, providing their coordinates. Figure 6 displays the spatial distribution of the top five flood-prone areas within the watershed. This map identifies the locations where maximum flooding occurred during the storm event, based on model predictions and observed data.

5.4. Model calibration

Finally, the model's performance was validated using data from a real storm that occurred on March 31, 2022. This storm data was collected from a rainfall station (Station No.: 118, Name: Beer Creek at US231) operated by NWFWMD, as shown in Figure 6. (https://nwfwmd.aquaticinformatics.net/Data/DataSet /Chart/Location/008571/DataSet/Precip/Recorder/Interval/AllData). Additionally, NWFWMD operates another station at the same location that records river stages during storm events. (https://nwfwmd.aquaticinformatics.net/Data/DataSet/Chart/Location/008571/DataSet/Stage/NAVD88/Interval/AllData).

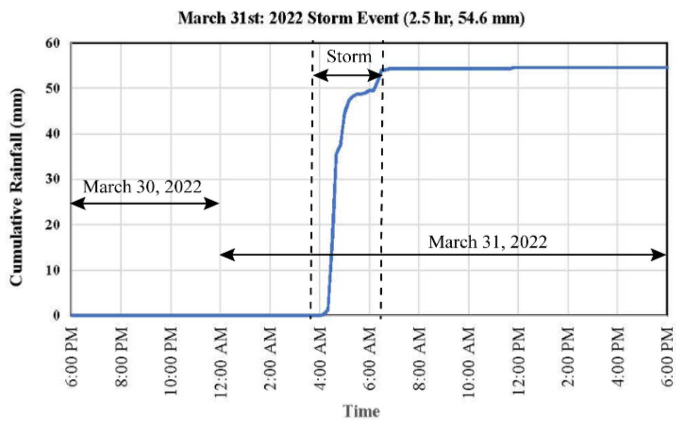

Figure 7. Storm Event of March 31, 2022.

Figure 7 illustrates the actual storm event on March 31, 2022, which lasted approximately 2.5 hours and produced 55 mm (2.15 inches) of rainfall. The storm's intensity and duration were key factors influencing the hydrologic response in the region. The observed rainfall data from this event was used to drive the hydrological model, which was subsequently applied to determine the stages for gage Station No. 118 at Beer Creek, as shown in the following figure (Figure 8).

Figure 8 compares the actual observed water stages with the model-predicted stages at the Beer-Creek gage station, showing the accuracy and reliability of the flood model for this location. As shown in Figure 8, the model-predicted results generally align with the actual (observed) time series data. Although the actual and model-predicted stages are close, Figure 8 indicates that the model slightly under-predicts the stages at Station No. 118. This discrepancy is likely due to the model's sensitivity to stage changes and flow rates associated with the connections between nodes. Despite this, it is clear that the model effectively predicts flood inundation levels at any given time.

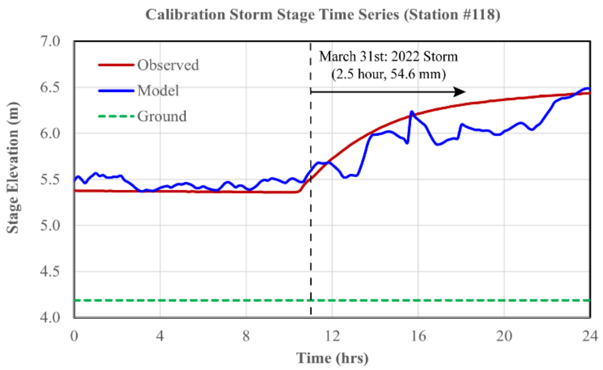

Figure 8. Comparison of observed and model-predicted stages at Beer-creek gage station (#118)

5.5. Discussion of Results

The experimental results highlight several key findings:

The significant increase (527 ha-m) in post-hurricane surface runoff, primarily driven by the conversion of mature evergreen forests to shrubland, underscores the importance of considering land cover changes when assessing flood risk. The higher runoff in the post-hurricane scenario suggests that the region is now more vulnerable to flooding, especially during intense storm events.

The 256% increase in the inundated areas demonstrates the lasting impact of Hurricane Michael on local hydrology. The larger flooded areas post-hurricane suggest that flood management strategies must be adapted to account for these changes and that more localized flooding may occur in areas previously thought to be less vulnerable.

The identification of specific flood-prone locations in the watershed provides valuable information for city planners and water resource managers. By targeting these vulnerable areas for flood mitigation measures, the region can reduce its overall flood risk.

While the model successfully predicted the general flood patterns and stages, the slight underprediction of flood stages indicates a need for further model refinement. The model's sensitivity to certain inputs, such as precipitation intensity and storm duration, suggests that improvements in data resolution and model calibration could enhance prediction accuracy, especially for extreme storm events.

6. Conclusions

This study provides valuable insights into the recurrent flooding challenges faced by Bay County, Florida, particularly in the aftermath of Hurricane Michael in 2018. Our research demonstrates that the hurricane significantly altered both surface and subsurface hydrological conditions, exacerbating flood vulnerability in the region. Specifically, the area subject to inundation for a 25-year, 24-hour design storm increased by 256% from pre-hurricane to post-hurricane conditions, underscoring the profound impact of the storm on the local hydrology. This dramatic increase highlights the urgent need to update and improve flood management plans, as current models may no longer be accurate in predicting flood risks under altered conditions.

The integration of satellite imagery and hydrological data into the modeling process proved essential for simulating realistic flood scenarios. This methodological approach enhanced the precision of flood inundation estimates, allowing us to identify flood-prone areas with greater accuracy. The model's ability to estimate flood stages, while slightly underestimating actual levels, still demonstrated a high degree of consistency with observed trends, particularly when compared to actual storm data from March 31, 2022. Although the model's predictions can be further refined, it serves as a valuable tool for city planners and policymakers in assessing flood risks and informing mitigation strategies.

While the current study offers important contributions, several areas remain for future investigation to further refine flood modeling and risk assessment in the region. One potential direction is the incorporation of finer spatial resolution in the hydrological model. This could help improve accuracy in regions with more complex topography or land-use changes that may not be adequately captured with the current mesh resolution. Additionally, more extensive calibration with long-term, real-time hydrological data could help reduce model uncertainties and improve flood stage predictions.

Another area for future research is exploration into the integration of real-time data streams, such as river gauge readings and meteorological data, which could improve the model's responsiveness to dynamic, evolving storm events. Real-time simulations may offer a more effective early warning system and enable more precise, timely interventions during flood events [10].

In conclusion, this study not only enhances our understanding of flood dynamics in the wake of natural disasters but also provides a framework for integrating modern data sources into hydrological models. The findings presented here lay the groundwork for future improvements in flood risk reduction strategies. By continuously refining these models and incorporating emerging data sources, we can develop more effective strategies to mitigate the impacts of future floods, better protecting vulnerable communities from the devastating effects of extreme weather events.

Declaration of Conflict of Interests

The authors declare that there is no conflict of interest. They have no known competing financial interests or personal relationships that could have appeared to influence the work reported in this paper.

Acknowledgment

This work was supported by grants from the Bay County (Florida, USA) Board of County Commissioners. The authors also thank Mr. Pete Singhofen and Mrs. Annamarie Singhofen for their support in providing access to ICPR. We would like to extend our sincere thanks to OpenAI for their ChatGPT tool (a large language model) for its assistance in language editing, enhancing the quality of the text, and supporting the writing of this manuscript.

References

[1.] Merwade V, Cook A, Coonrod J. GIS techniques for creating river terrain models for hydrodynamic modeling and flood inundation mapping. Environ. Modell. Softw. 2008;23 (10-11): 1300-1311.

[2.] Saksena1 S, Merwade V. Integrated Modeling of Surface-Subsurface Processes to Understand River- Floodplain Hydrodynamics in the Upper Wabash River Basin. World Environmental and Water Resources Congress, ASCE, 2017.

[3.] Afshari S, Tavakoly AA, Rajib MA, Zheng X, Follum ML, Omranian E, Fekete BM. Comparison of new generation low-complexity flood inundation mapping tools with a hydrodynamic model. J. Hydrol. 2018; 556:539-556.

[4.] Alfieri L, Salamon P, Bianchi A, Neal J, Bates P, Feyen L. Advances in Pan-European flood hazard mapping, Hydrol. Process. 2014;28(13): 4067-4077.

[5.] Liu B, Li X, Zheng G. Coastal Inundation Mapping from Bitemporal and Dual-Polarization SAR Imagery Based on Deep Convolutional Neural Networks. J. Geophys. Res. Oceans. 2019;124 (12) 9101-9113.

[6.] Cook A, Merwade V. Effect of topographic data, geometric configuration and modeling approach on flood inundation mapping. J. Hydrol. 2009; 377 (1-2):131-142.

[7.] Saksena S, Merwade V, Singhofen PJ. Flood inundation modeling and mapping by integrating surface and subsurface hydrology with river hydrodynamics. J. Hydrol. 2019; 575:1155-1177.

[8.] Streamline Technologies, 2018. ICPR4 Technical Reference Manual. Streamline Technology Inc., Winter Springs. Florida.

[9.] Ahmad H, Miller JW, George RD. Minimizing pond size using an off-site pond in a closed basin: A storm flow mitigation design and evaluation. IJSDP. 2014; 9:211–224.

[10.] OpenAI. (2023). *ChatGPT* (4.0 version) [Large language model]

[11.] USDA. “Technical Release 55,” Natural Resources Conservation Service, June, 1986. https://www.hydrocad.net/pdf/TR-55%20Manual.pdf

How to Cite This Article

Ahmad, H., and Vickers, W., Impact of Natural Disasters on Flooding: An Assessment Using Satellite Data and Surface-Subsurface Modeling, Journal of Nature, Science & Technology, 4(2024), 4949. https://doi.org/10.36937/ben.2024.4949.